Momentum reconstruction and contact of the one-dimensional Bose-Fermi mixture

Ovidiu I. Pâţu[1] and Andreas Klümper[2]
[1]*Institute for Space Sciences, Bucharest-Măgurele 077125, Romania*
[2]*Fakultät für Mathematik und Naturwissenschaften, Bergische Universität Wuppertal, 42097 Wuppertal, Germany*

(Received 21 November 2018; published 30 January 2019)

We investigate the one-dimensional mixture of scalar bosons and spin-polarized fermions interacting through a δ-function potential. Using a thermodynamic description derived by employing a lattice embedding of the continuum model and the quantum transfer-matrix method, we perform a detailed analysis of the contact and quantum critical behavior. We show that the compressibility Wilson ratio presents anomalous enhancement at the quantum critical points and that the boundaries of the quantum critical regions can be well mapped by the maxima of the specific heat. As a function of the coupling strength and temperature, the contact presents nonmonotonic behavior. In the strong-coupling regime the local minimum exhibited by the contact as a function of temperature is accompanied by a significant momentum reconstruction at both low and high momenta. This momentum reconstruction occurs as the system crosses the boundary between the Tomonaga-Luttinger liquid phase to the spin-incoherent regime and provides an experimental signature of the transition.

DOI: 10.1103/PhysRevA.99.013628

I. INTRODUCTION

Physical systems of ultracold atomic gases are characterized by a high degree of control over interaction strength, statistics and dimensionality, which makes them ideal candidates for the investigation of various quantum many-body phenomena [1–3]. The absence of defects and impurities makes these systems particularly suited for the simulation of many condensed-matter models, but at the same time they also allow for the creation of more exotic quantum systems. One example is the degenerate mixture of bosons and fermions which has been experimentally realized in various trap and lattice geometries. The study of Bose-Fermi mixtures (BFMs) is extremely important from an experimental point of view due to the sympathetic cooling of fermions via interactions with bosons [4] but also theoretically because they exhibit phases and phenomena which are seldom studied in the condensed-matter context. One-dimensional BFMs, which are characterized by enhanced quantum fluctuations, have been investigated, on both the lattice and the continuum, using mean-field theory [5–8], bosonization [Tomonaga-Luttinger liquid (TLL)] [9–15], density waves [16,17], exact solutions [18–32], and various numerical approaches [33–41]. The phase diagram is very rich and contains Mott insulators, spin- and charge-density waves, phase separation, Tomonaga-Luttinger and spin-incoherent liquids, and Wigner crystals. In recent years there has also been an increasing number of studies on few-body mixtures, which are in general focused on the strong-coupling regime. Various methods are employed such as the multicomponent generalization of the Bose-Fermi mapping [42–51], approximation by spin chains [52–54], energy-functional techniques [55–58], and trial wave functions [59–61].

In this article we study the one-dimensional (1D) mixture of scalar bosons and spin-polarized fermions with contact interactions in the continuum. This system has been investigated in several papers, but the vast majority of them were restricted to the study of the ground state. However, experiments are performed at finite temperature, which highlights the need for the computation of accurate thermodynamic data. For example, many multicomponent systems present quantum phase transitions (QPTs) at zero temperature [62] as certain parameters are varied (pressure, magnetic field, doping, etc.). The effects of these QPTs can also be detected at finite temperature in the so-called quantum critical (QC) region, which is characterized by strong coupling of the thermal and quantum fluctuations. While the zero-temperature phase diagram gives the quantum critical points, the determination of the boundaries of the QC regions can be done only by computing the thermodynamic properties.

The 1D BFM with contact interactions is integrable when the masses of the fermions and bosons and all the coupling strengths are independently equal [18,24–26]. In this case, powerful methods associated with the Bethe ansatz [63,64] can be employed to calculate various zero- and finite-temperature properties. In particular, the thermodynamics of the system can be derived using the thermodynamic Bethe ansatz (TBA) [65,66]. In general, thermodynamic descriptions of integrable models derived using the TBA are characterized by an infinite number of integral equations [66], which makes their numerical implementation very difficult. While the BFM is one of the very few exceptions from this rule [27], the TBA thermodynamics of a large number of integrable multicomponent systems like the two-component Fermi gas (2CFG) [67,68] or two-component Bose gas (2CBG) [67] suffer from the same drawback. Other notable exceptions are systems characterized by q-deformed algebras at special roots of unity, which quite typically lead to a truncation. One way of circumventing these difficulties is provided by the quantum transfer-matrix (QTM) method [69–74], which has the advantage of producing a finite number of integral equations that are easier to implement numerically. In Refs. [75–77]

 ©2019 American Physical Society

we succeeded in deriving such thermodynamic descriptions for the 2CBG and 2CFG and in this article we show that the same method can also applied in the case of the Bose-Fermi mixture. Our result hints strongly that similar efficient thermodynamic descriptions involving only κ integral equations for a κ-component system can be derived using the same method.

We use this result to perform a detailed analysis of the universal Tan contact [78–91] which governs the $1/k^4$ of the momentum distribution. At finite temperature and as a function of the coupling strength, the contact presents local maxima for small values of the boson fraction, a feature which is not present at zero temperature. Even more interesting, the contact develops a local minimum as a function of the temperature, which results in a counterintuitive momentum reconstruction at the system's transition from the TLL phase to the incoherent regime. In addition, we determine the boundaries of the quantum critical regions which can be identified with the maxima of the grand-canonical specific heat. Similar to the case of the 2CBG [92], the Wilson ratio presents anomalous enhancement in the vicinity of the quantum critical points and can be used to distinguish between different phases.

The plan of the paper is as follows. In Sec. II we introduce the model and in Sec. III we present the TBA thermodynamics and our results derived in the quantum transfer-matrix framework. The analysis of the contact and momentum reconstruction is presented in Sec. IV and the determination of the boundaries of the QC regions is performed in Sec. V. The derivation of the thermodynamics is outlined in Secs. VI and VII. We summarize in Sec. VIII.

II. MODEL

The model investigated in this article describes one-dimensional scalar bosons and spinless fermions with contact interactions. The Hamiltonian in second quantization is

$$H = \int dx \sum_{\sigma\in\{B,F\}} \left(\frac{\hbar^2}{2m_\sigma} \partial_x \Psi_\sigma^\dagger \partial_x \Psi_\sigma - \mu_\sigma \Psi_\sigma^\dagger \Psi_\sigma \right) + \frac{g_{BB}}{2} \Psi_B^\dagger \Psi_B^\dagger \Psi_B \Psi_B + g_{BF} \Psi_B^\dagger \Psi_F^\dagger \Psi_F \Psi_B, \tag{1}$$

where $\Psi_B(x)$ and $\Psi_F(x)$ are bosonic and fermionic fields satisfying canonical commutation and anticommutation relations, m_B and m_F are the masses of the bosonic and fermionic particles, and μ_B and μ_F are the chemical potentials. In (1), g_{BB} and g_{BF} are the Bose-Bose and Bose-Fermi interaction strengths which can be expressed in terms of the 1D scattering lengths a_{BB} and a_{BF} via $g_{\sigma\sigma'} = -\hbar^2/m_{\sigma\sigma'}a_{\sigma\sigma'}$, with $\sigma, \sigma' \in \{B, F\}$ and $m_{\sigma\sigma'} = (m_\sigma + m_{\sigma'})/m_\sigma m_{\sigma'}$ the reduced mass.

The Hamiltonian (1) is integrable when the masses $m_B = m_F = m$ and coupling strengths are equal $g_{BB} = g_{BF} = g$ [18,24,25]. This is the case that will be considered in the rest of this article and in order to correspond to the literature we are going to use units of $\hbar = 2m = 1$ and introduce $g = 2c$ with $c > 0$. For a system of M particles, of which M_B are bosons and $M_F = M - M_B$ are fermions, the energy spectrum of (1) is [24,25]

$$E_{BF} = \sum_{j=1}^{M} \left(k_j^{(1)}\right)^2 - \mu_B M_B - \mu_F (M - M_B), \tag{2}$$

with $\{k_j^{(1)}\}_{j=1}^M$ satisfying the Bethe ansatz equations (BAEs)

$$e^{ik_s^{(1)} L_{BF}} = \prod_{p=1}^{M_B} \frac{k_s^{(1)} - k_p^{(2)} + ic/2}{k_s^{(1)} - k_p^{(2)} - ic/2}, \quad s = 1, \ldots, M, \tag{3a}$$

$$1 = \prod_{j=1}^{M} \frac{k_l^{(2)} - k_j^{(1)} + ic/2}{k_l^{(2)} - k_j^{(1)} - ic/2}, \quad l = 1, \ldots, M_B, \tag{3b}$$

where L_{BF} is the length of the system and we have assumed periodic boundary conditions.

III. THERMODYNAMICS

A. The TBA result

From a historical point of view, the first method employed to determine the thermodynamics of an integrable model was the thermodynamic Bethe ansatz [66] introduced by Yang and Yang in their study of the Lieb-Liniger model [65]. In the TBA framework the Bose-Fermi mixture was investigated in Ref. [27]. Introducing an effective magnetic field and chemical potential defined by $\mu = (\mu_B + \mu_F)/2$ and $2H = \mu_B - \mu_F$, the grand canonical potential per length is ($\beta = 1/T$)

$$\phi_{YCZ}(\mu, H, \beta) = -\frac{1}{2\pi\beta} \int_{\mathbb{R}} \ln[1 + e^{-\beta\epsilon(k)}] dk, \tag{4}$$

with $\epsilon(k)$ satisfying the system of nonlinear integral equations (NLIEs)

$$\epsilon(k) = k^2 - \mu + H - \beta^{-1} \int_{\mathbb{R}} b_1(k - \lambda) \ln[1 + e^{-\beta\varphi(\lambda)}] d\lambda,$$

$$\varphi(\lambda) = -2H - \beta^{-1} \int_{\mathbb{R}} b_1(\lambda - k) \ln[1 + e^{-\beta\epsilon(k)}] dk,$$

with $b_1(k) = c/2\pi(c^2/4 + k^2)$. It should be noted that in general the TBA description of multicomponent systems involves an infinite number of NLIEs. Therefore, it is extremely fortunate that in the case of the BFM we encounter only two equations, which is due to the fact that the Bethe equations (3) have only real solutions. However, in the case of all the other multicomponent systems with contact interactions like the 2CBG and 2CFG and even many single-component systems, the Bethe equations have complex solutions, which means that the TBA description is very hard to implement numerically. A more efficient method which has the advantage of producing only a finite number of integral equations even for models whose BAEs admit complex solutions is the QTM technique. Even though the QTM can be defined only for lattice models, this difficulty can be circumvented by considering a lattice embedding for the continuum model. In Refs. [75–77] we employed this method and succeeded in deriving a system of only two NLIEs characterizing the thermodynamics of the 2CBG and 2CFG. The same method can be used in the case of the Bose-Fermi mixture, as we will show below.

B. Alternative thermodynamic description

The lattice embedding of the BFM is the Perk-Schultz spin chain with the $(-+-)$ grading (see Sec. VI). The derivation of the QTM thermodynamic description is relatively involved

and will be presented in Sec. VII. Here we present the main result and show the equivalence with the TBA description. The grand-canonical potential per length is

$$\phi(\mu, H, \beta) = -\frac{1}{2\pi\beta}\int_{\mathbb{R}} [\ln A_1(k) + \ln A_2(k)]dk, \quad (5)$$

with the two auxiliary functions $a_{1,2}(k)$ $[A_{1,2}(k) = 1 + a_{1,2}(k)]$ satisfying the system of NLIEs

$$\ln a_1(k) = -\beta(k^2 - \mu - H) + \int_{\mathbb{R}} K_0(k-k')\ln A_1(k')dk' + \int_{\mathbb{R}+i\varepsilon} K_2(k-k')\ln A_2(k')dk', \quad (6a)$$

$$\ln a_2(k) = -\beta(k^2 - \mu + H) + \int_{\mathbb{R}-i\varepsilon} K_1(k-k')\ln A_1(k')dk', \quad (6b)$$

where $\varepsilon \to 0$ and the kernels are defined by $K_0(k) = \frac{1}{2\pi}\frac{2c}{k^2+c^2}$, $K_1(k) = \frac{1}{2\pi}\frac{c}{k(k+ic)}$, and $K_2(k) = \frac{1}{2\pi}\frac{c}{k(k-ic)}$.

We can analytically check the validity of our results in some particular cases. In the noninteracting limit $c \to 0$, using $\lim_{c\to 0} K_1(k + i\varepsilon) = \lim_{c\to 0} K_2(k - i\varepsilon) = 0$ and $\lim_{c\to 0} K_2(k) = \delta(k)$, the NLIEs (6) decouple

$$\ln a_1(k) = -\beta(k^2 - \mu - H) + \ln[1 + a_1(k)],$$
$$\ln a_2(k) = -\beta(k^2 - \mu + H)$$

and can be solved, obtaining for the grand-canonical potential $\phi(\mu, H, \beta) = \frac{1}{2\pi\beta}\int_{\mathbb{R}} \ln[1 - e^{-\beta(k^2-\mu-H)}]dk - \frac{1}{2\pi\beta}\int_{\mathbb{R}} \ln[1 + e^{-\beta(k^2-\mu+H)}]dk$, which is the known result for a noninteracting mixture of fermions and bosons with different chemical potentials. For large values of H the fermionic degrees of freedom are strongly suppressed, $a_2(k) \sim 0$. Equations (6) reduce to the Yang-Yang equation for the Lieb-Liniger model [65]

$$\ln a_1(k) = -\beta(k^2 - \mu - H) + \int_{\mathbb{R}} K_0(k-k')\ln A_1(k')dk'$$

and $\phi(\mu, H, \beta) = -\frac{1}{2\pi\beta}\int_{\mathbb{R}} \ln[1 + a_1(k)]dk$, which reproduces the TBA result for single-component bosons with contact interactions. In the impenetrable limit $c \to \infty$ our result should coincide with the one obtained by Takahashi for two-component impenetrable fermions, i.e.,

$$\phi_\infty(\mu, H, \beta) = -\frac{1}{2\pi\beta}\int_{\mathbb{R}} \ln[1 + 2\cosh(\beta H)e^{-\beta(k^2-\mu)}]dk. \quad (7)$$

While we have not succeeded in proving analytically the equivalence of our result with (7), we have checked it numerically and found perfect agreement.

The equivalence of the TBA and QTM thermodynamic descriptions is shown in Fig. 1, where we plot the numerically evaluated relative error defined as

$$\Delta|\phi - \phi_{YCZ}| = \frac{|\phi - \phi_{YCZ}|}{\max[\phi, \phi_{YCZ}]}, \quad (8)$$

which shows that (4) and (5) (modulo numerical errors) produce identical results. Because in both cases we have

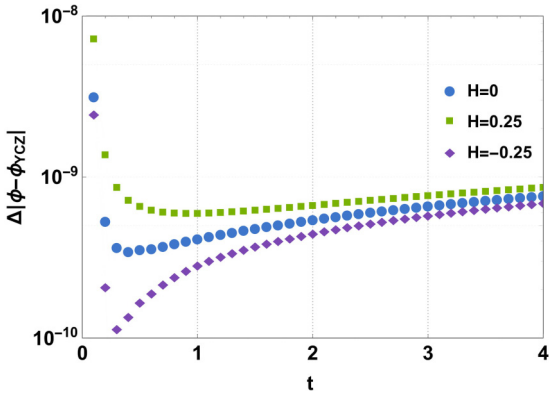

FIG. 1. Plot of the relative errors between the TBA grand-canonical potential (4) and our result (5) for $c = 1$ and $H = -0.25$, 0, 0.25. Here $t = T/c^2$.

$\phi(c, \mu, H, T) = c^3\phi(1, \mu/c^2, H/c^2, T/c^2)$, it is sufficient to consider only $c = 1$. The computational complexities of both descriptions are the same, which means that choosing one of them is a matter of personal choice. In the rest of the paper we use (5) and (6) mainly because our auxiliary functions have zero asymptotics at infinity, resulting in a more precise treatment of convolutions using the fast Fourier transform.

The thermodynamic descriptions for the 2CBG [75,76], 2CFG [77], and BFM, (4) and (6), derived in the quantum transfer-matrix framework, involve only two auxiliary functions $a_{1,2}(k)$ and the same expression for the grand-canonical potential (5). The system of NLIEs is different in each case and can be compactly written as $([f * g](x) = \int_{\mathbb{R}} f(x-x')g(x')dx')$

$$\begin{pmatrix}\ln a_1(k)\\ \ln a_2(k)\end{pmatrix} = \begin{pmatrix}d_1(k)\\ d_2(k)\end{pmatrix} + \mathbf{K} * \begin{pmatrix}\ln A_1(k)\\ \ln A_2(k)\end{pmatrix}, \quad (9)$$

with $d_j(k) = -\beta[k^2 + \mu + (-1)^j H]$ and kernel matrices

$$\mathbf{K}_{BB} = \begin{pmatrix}K_0 & K_2\\ K_1 & K_0\end{pmatrix}, \quad \mathbf{K}_{FF} = \begin{pmatrix}0 & K_2\\ K_1 & 0\end{pmatrix} \quad (10)$$

for the 2CBG and 2CFG and

$$\mathbf{K}_{BF} = \begin{pmatrix}K_0 & K_2\\ K_1 & 0\end{pmatrix} \quad (11)$$

for the Bose-Fermi mixture. It is therefore tempting to conjecture that the thermodynamics of a three-component system with contact interactions can be described by three auxiliary functions $a_i(k)$ $(i = 1, 2, 3)$, $A_i(k) = 1 + a_i(k)$, with grand-canonical potential

$$\phi(\{\mu_i\}_{i=1}^3, \beta) = -\frac{1}{2\pi\beta}\int_{\mathbb{R}} \ln A_1(k) + \ln A_2(k) + \ln A_2(k)dk,$$

and $a_i(k)$ satisfying

$$\begin{pmatrix}\ln a_1(k)\\ \ln a_2(k)\\ \ln a_3(k)\end{pmatrix} = \begin{pmatrix}d_1(k)\\ d_2(k)\\ d_3(k)\end{pmatrix} + \mathbf{K} * \begin{pmatrix}\ln A_1(k)\\ \ln A_2(k)\\ \ln A_3(k)\end{pmatrix}, \quad (12)$$

with $d_j(k) = -\beta(k^2 + \mu_j)$. In the case of a three-component bosonic and fermionic system we conjecture that the kernels

are

$$\mathbf{K}_{BBB} = \begin{pmatrix} K_0 & K_2 & K_2 \\ K_1 & K_0 & K_2 \\ K_1 & K_1 & K_0 \end{pmatrix}, \quad \mathbf{K}_{FFF} = \begin{pmatrix} 0 & K_2 & K_2 \\ K_1 & 0 & K_2 \\ K_1 & K_1 & 0 \end{pmatrix}$$

and in the case of the Bose-Bose-Fermi and Bose-Fermi-Fermi mixtures the kernels are

$$\mathbf{K}_{BBF} = \begin{pmatrix} K_0 & K_2 & K_2 \\ K_1 & K_0 & K_2 \\ K_1 & K_1 & 0 \end{pmatrix}, \quad \mathbf{K}_{BFF} = \begin{pmatrix} K_0 & K_2 & K_2 \\ K_1 & 0 & K_2 \\ K_1 & K_1 & 0 \end{pmatrix}.$$

These conjectured thermodynamic descriptions present the correct limits when $c \to 0$ and when one of the components is suppressed, however a definitive proof of their validity requires the numerical checking with the TBA predictions. This is beyond the scope of the present paper.

IV. CONTACT

The momentum distribution of 1D models with contact interactions present a universal $n(k) \sim \mathcal{C}/k^4$ decay [81,90,91]. The universal coefficient $\mathcal{C}$ which governs the asymptotic behavior is called the contact and appears in a series of identities involving macroscopic properties of the system which are called Tan relations [78–91]. The $1/k^4$ decay and the Tan relations are valid also for nonintegrable systems in the presence of a trapping potential, at zero or finite temperature, and for few- or many-body systems. For the BFM the bosonic and fermionic contacts are given by [51,91]

$$\mathcal{C}_B = c^2(\langle \Psi_B^\dagger \Psi_B^\dagger \Psi_B \Psi_B \rangle + \langle \Psi_B^\dagger \Psi_F^\dagger \Psi_F \Psi_B \rangle),$$
$$\mathcal{C}_F = c^2 \langle \Psi_B^\dagger \Psi_F^\dagger \Psi_F \Psi_B \rangle.$$

Even though the individual contacts are hard to compute, the total contact can be derived from the thermodynamics of the system using the Hellmann-Feynman theorem [91]

$$\mathcal{C} = \mathcal{C}_B + \mathcal{C}_F = c^2 \left(\frac{\partial \phi}{\partial c} \right)_{\mu,H,T}. \tag{13}$$

A. Contact at zero temperature

At zero temperature the thermodynamics of the system is described by a system of Fredholm integral equations which can be derived from the BAEs (3) [24,25],

$$\rho_c(k) = \frac{1}{2\pi} + \int_{-\lambda_0}^{\lambda_0} b_1(k-\lambda)\rho_s(\lambda)d\lambda, \tag{14a}$$

$$\rho_s(\lambda) = \int_{-k_0}^{k_0} b_1(\lambda - k)\rho_c(k)dk. \tag{14b}$$

Here k_0 and λ_0 are two parameters which set the total density $n = M/L_{BF}$ and the boson fraction $\alpha = M_B/L_{BF}$ via $n = \int_{-k_0}^{k_0} \rho_c(k)dk$ and $\alpha = \int_{-\lambda_0}^{\lambda_0} \rho_s(\lambda)d\lambda$. The energy density of the system is $\mathcal{E} = \int_{-k_0}^{k_0} k^2 \rho_c(k)dk$. It is useful to introduce the dimensionless coupling strength $\gamma = c/n$. The system is in the Tonks-Girardeau regime when $\gamma \gg 1$ and weakly interacting when $\gamma \ll 1$.

Once we have computed the energy density, the total contact can be derived from Eq. (13), which at zero temperature takes the form

$$\mathcal{C} = n\gamma^2 \left(\frac{\partial \mathcal{E}}{\partial \gamma} \right)_{n,\alpha}. \tag{15}$$

In general, it is relatively easy to derive approximate expressions for the energy in the strong-coupling limit [24,25,51]

$$\mathcal{E}_S(\gamma,\alpha) \underset{\gamma\gg1}{\sim} \frac{n^3\pi^2}{3}\left[1 - \frac{4}{\gamma}\left(\alpha + \frac{\sin\pi\alpha}{\pi}\right) + \frac{12}{\gamma^2}\left(\alpha + \frac{\sin\pi\alpha}{\pi}\right)^2\right]; \tag{16}$$

however, in the weakly interacting limit serious difficulties are encountered due to the fact that the $b_1(k)$ kernel becomes a δ function. In this limit only the first term of the asymptotic expansion was obtained [5]

$$\mathcal{E}_W(\gamma,\alpha) \underset{\gamma\ll1}{\sim} n^3\left[\frac{\pi^2}{3}(1-\alpha)^3 + 2\gamma\alpha - \gamma\alpha^2\right]. \tag{17}$$

One way in which we can improve this approximate expression is to replace the γ terms which are multiplied with powers of the boson fraction with the weak-coupling expansion of the Lieb-Liniger model [93–97] $\mathcal{E}_{\rm LL}(\gamma) \underset{\gamma\ll1}{\sim} \gamma - \frac{4}{3\pi}\gamma^{3/2} + (\frac{1}{6} - \frac{1}{\pi^2})\gamma^2$, obtaining

$$\mathcal{E}_{WI}(\gamma,\alpha) \underset{\gamma\ll1}{\sim} n^3\left[\frac{\pi^2}{3}(1-\alpha)^3 + 2\mathcal{E}_{\rm LL}(\gamma)\alpha - \mathcal{E}_{\rm LL}(\gamma)\alpha^2\right]. \tag{18}$$

This expression reduces to the free fermionic result for $\alpha = 0$ and reproduces the Lieb-Liniger expansion when the system is purely bosonic ($\alpha = 1$). In the top row of Fig. 2 we present results for the normalized energy density computed using (14) together with the asymptotic expansions at strong and weak coupling. The insets show that (18) represents a significant improvement over (17) and for $\alpha > 0.5$ the asymptotic expansions are valid for almost all values of the coupling strengths. The dimensionless contact $s = \mathcal{C}/(\pi n)^4$ calculated using (15) is shown in the bottom row of Fig. 2. At zero temperature the contact is a monotonically increasing function of both the coupling constant and bosonic fraction.

B. Contact at finite temperature

At finite temperature we use (5), (6), and (13) for the determination of the contact. The dependence of the contact on the coupling strength for $\tau = 0, 1.3, 4$ with $\tau = T/n^2$ and different boson fractions is shown in Fig. 3. We distinguish two notable features. First, for small values of the boson fraction, $\alpha = 0.05$ and $\alpha = 0.2$, the contact at finite temperatures develops a local maximum which is more pronounced at low temperatures. Second, with the exception of the system close to the purely bosonic case $\alpha = 1$, for large values of the coupling strength the contact at zero temperature is larger than the one at finite temperature. This is rather counterintuitive if we remember that the contact governs the long tail of the momentum distribution. Therefore, a smaller contact at higher temperature means that as we increase T the number of particles with large momenta decreases compared with the ground state. This phenomenon can be seen more clearly in

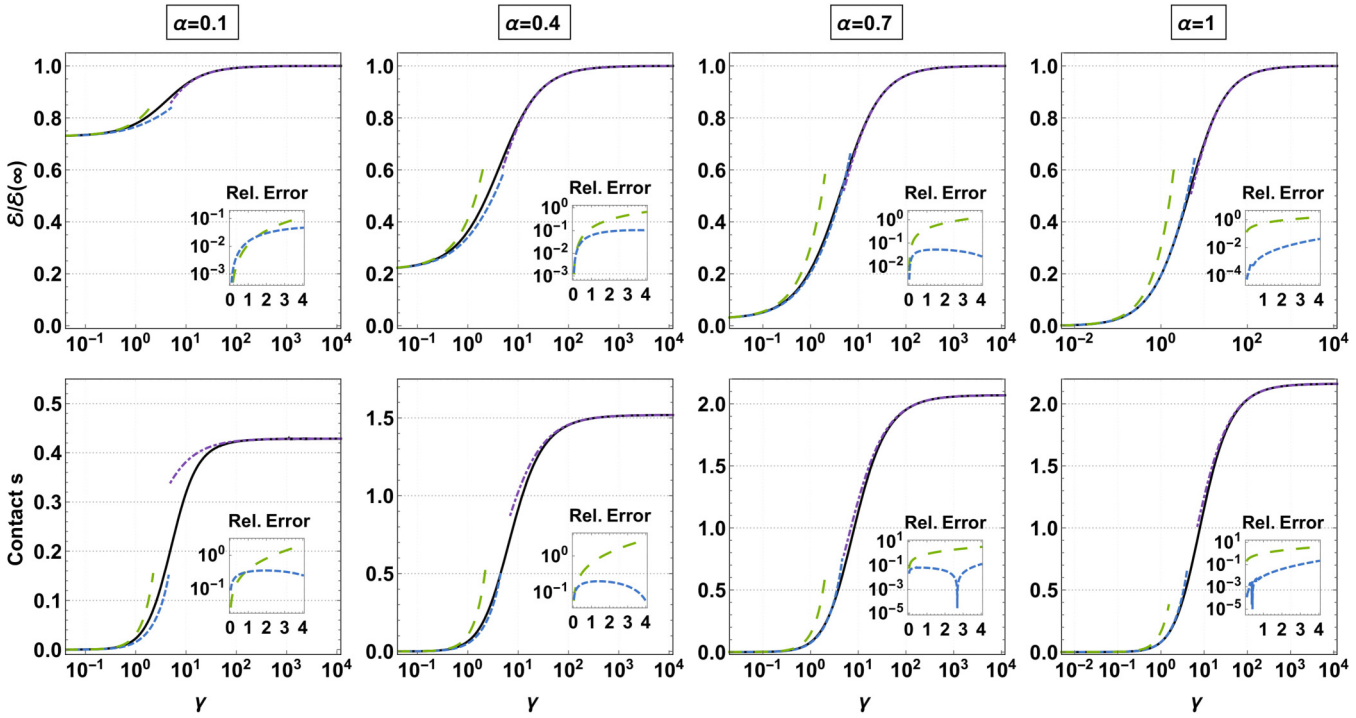

FIG. 2. The top row shows the energy density normalized by $\mathcal{E}(\infty) = n^3\pi^2/3$ (black solid line) as a function of the dimensionless coupling strength γ for several values of the boson fraction. Also plotted are the strong- and weak-coupling approximations given by Eq. (16) (violet dash-dotted line), Eq. (17) (green long-dashed line), and Eq. (18) (blue short-dashed line). The insets contain the relative errors $|\mathcal{E} - \mathcal{E}_{W,WI}|/\max[\mathcal{E}, \mathcal{E}_{W,WI}]$ of the weak-coupling expansions which show that (18) is an improved approximation. The density is fixed at $n = 1/2$. The bottom row shows the normalized total contact $s = \mathcal{C}/(\pi n)^4$ as a function of the coupling strength derived from the expressions for the energy and approximations using Eq. (15). The insets contain the relative errors of the contacts derived from the two weak-coupling expansions.

Fig. 4, where we present the dependence of the contact on the reduced temperature for moderate and strong coupling. For $\gamma = 2$ the contact is a monotonically increasing function of the temperature for all values of the boson fraction; however, at strong coupling the contact develops a pronounced minimum, the only exception being the case of $\alpha = 1$. This momentum reconstruction at low temperatures is a feature of 1D multicomponent systems being present also in the case of the two-component Fermi [77] and Bose [92] gas and serves as a signature of the transition from the Tomonaga-Luttinger liquid

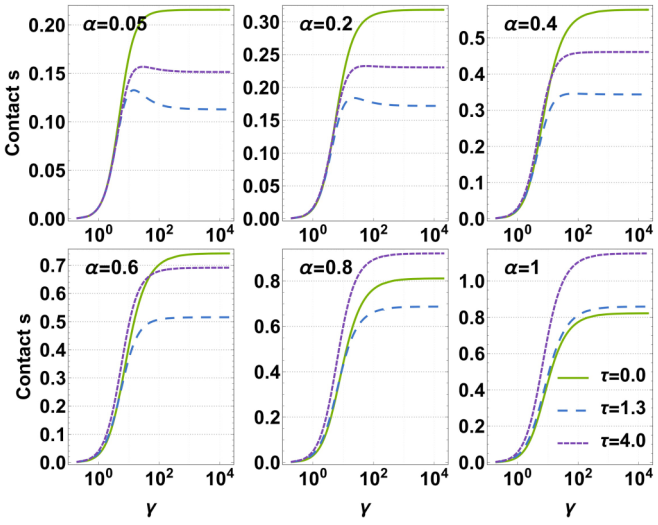

FIG. 3. Dependence of the dimensionless contact on the coupling strength γ for several values of the reduced temperature ($\tau = T/n^2$, with $n = 1/2$) and different boson fractions. Compared with the ground state, the contact develops a local maximum for small values of α, which is more pronounced at low but finite temperatures.

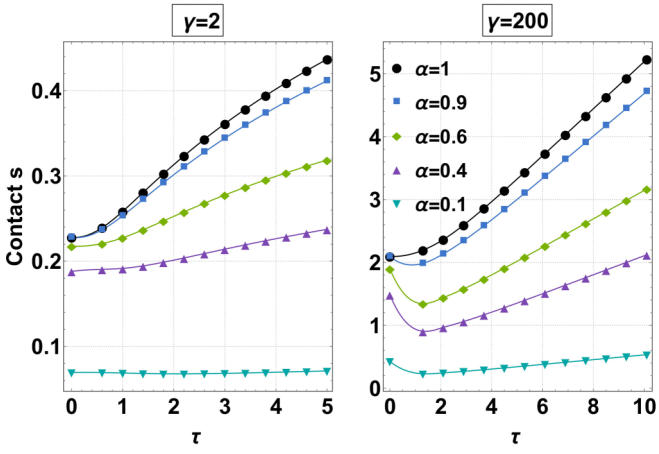

FIG. 4. Dependence of the dimensionless contact on the reduced temperature for $\gamma = 2$ and $\gamma = 200$. At strong coupling the contact presents a pronounced minimum for all values of the boson fraction except $\alpha = 1$.

phase to the spin-incoherent regime. In 1D two-component systems there are two relevant temperature scales [98]: the Fermi temperature $T_F = \pi^2 n^2$, which characterizes the charge degrees of freedom, and $T_0 = E_F/\gamma$, which estimates the bandwidth of the spin excitations (in our case a spin excitation is represented by the removal of a fermion and the addition of a boson in the system). In the strong-coupling limit we have $0 \ll T_0 \equiv E_F/\gamma \ll E_F$ and for $T \in (T_0, T_F)$ the charge degrees of freedom are effectively frozen while the spin degrees of freedom are highly excited. This regime is called spin incoherent [99–103] and its properties are significantly different from the more well known Tomonaga-Luttinger liquid phase. In the BFM the minima of the contact at the transition indicate that the momentum distribution becomes narrower, but it is also easy to see that this is also accompanied by significant changes at low momenta. In the TLL regime the Bose-Bose field correlator presents algebraic decay with $\langle \Psi_B^\dagger(x)\Psi_B(0)\rangle \sim 1/|x|^{-1/2K_b}$, with $K_b = 1/[(\alpha-1)^2 - 1]$ derived by Frahm and Palacios [11] and numerically confirmed in [25]. Therefore, the bosonic momentum distribution will have a singularity at $k = 0$ of the type $n_B(k) \sim 1/|k|^{-1+1/2K_b}$. However, in the spin-incoherent regime the correlators are exponentially decaying, which means that the momentum distribution at zero becomes finite. This shows that there is a significant momentum reconstruction at both low and high momenta at the transition between the TLL and spin-incoherent regime.

V. BOUNDARIES OF THE QUANTUM CRITICAL REGIONS

In the vicinities of the quantum critical points (QCPs) the thermodynamics of the system is universal and is determined by the universality class of the quantum phase transition. If we keep the magnetic field fixed and consider the chemical potential as the driving parameter, in the quantum critical region the pressure can be written as [104]

$$p(\mu, H, T) \sim p_r(\mu, H) + T^{d/z+1}\mathcal{P}_H\left(\frac{\mu - \mu_c(H)}{T^{1/\nu z}}\right), \quad (19)$$

with p_r the regular part of the pressure, d the dimension, $\mathcal{P}_H$ a universal function, and $\mu_c(H)$ the quantum critical point. The universality class of the transition is determined by the correlation length exponent ν and the dynamical critical exponent z. All the other thermodynamic quantities can be derived from (19). For example, the density and compressibility, which are defined by $n = \partial p/\partial\mu$ and $\kappa = \partial^2\phi/\partial\mu^2$, are

$$n(\mu, H, T) \sim \frac{\partial p_r}{\partial\mu}(\mu, H) + T^{d/z+1-1/\nu z}\mathcal{P}'_H\left(\frac{\mu - \mu_c(H)}{T^{1/\nu z}}\right),$$

$$\kappa(\mu, H, T) \sim \frac{\partial^2 p_r}{\partial\mu^2}(\mu, H) + T^{d/z+1-2/\nu z}\mathcal{P}''_H\left(\frac{\mu - \mu_c(H)}{T^{1/\nu z}}\right).$$

We can determine the universality class of the transition by choosing certain values for z and ν and plotting the scaled pressure $(p - p_r)T^{-d/z-1}$ for several values of temperature [104]. If we have chosen the exponents correctly, all the curves will intersect at the value of the QCP $\mu_c(H)$. If we plot the scaled pressures as a function of $[\mu - \mu_c(H)]/T^{1/\nu z}$, all the curves should collapse to the universal curve $\mathcal{P}_H$.

A problem of considerable importance, both theoretically and experimentally, is the determination of the boundaries of the critical regions (CRs). The properties of the system in the CR are fundamentally different from the ones of other low-temperature phases and are characterized by the strong coupling of quantum and thermal fluctuations. In [92,105–107] it was argued that the grand canonical specific heat $c_V = -T\partial^2\phi/\partial T^2$ can be used to determine the boundaries of the QC regions with great precision. This is due to the fact that the grand-canonical specific heat is related to both the energy and number of particles fluctuations via $k_B T^2 c_v = \langle\delta(E - \mu N)^2\rangle$, which means that the QC boundaries can be identified with the local maxima of this quantity. Another important quantity which can be used to identify the low-temperature phases is the compressibility Wilson ratio [92,108,109] defined by

$$R_W^\kappa = \frac{\pi^2 k_B^2}{3} T \frac{\kappa}{c_V}, \quad (20)$$

with κ the compressibility. Because $k_B T\kappa = \langle\delta N^2\rangle$, the Wilson ratio will be almost constant in the low-temperature phases and will present anomalous enhancement in the QC regions and will scale like [108]

$$R_W^\kappa \sim \mathcal{Q}_H\left(\frac{\mu - \mu_c(H)}{T^{1/\nu z}}\right) + w_0 T^{1/2}\mathcal{F}_H\left(\frac{\mu - \mu_c(H)}{T^{1/\nu z}}\right). \quad (21)$$

Here $\mathcal{Q}_H$ and $\mathcal{F}_H$ are two universal functions, w_0 is a constant, and the second term on the right-hand side appears only if p_r is nonzero.

The quantum critical points and the phase diagram at zero temperature were determined in [31].[1] The number of QCPs depends on the sign of the magnetic field. For $H > 0$ we have only a QPT from the vacuum to a single-component TLL with critical point $\mu_c = -H$. In Fig. 5(a) we present results for the dependence of the grand-canonical specific heat on temperature and chemical potential for $H = 0.25$ and coupling strength $c = 1$. The specific heat presents two lines of local maxima fanning out from the QCP which separate the vacuum (classical gas) and the TLL phase from the QC region. The Wilson ratio, depicted in Fig. 5(b), is zero in the classical gas phase, presents a local maximum in the QC region, and is slowly increasing in the TLL phase. In this case $p_r \sim 0$ and R_W^κ obeys the scaling relation (19) with only the first term on the right-hand side. The scaling and collapse of the curves to the universal function $\mathcal{Q}_H$ are realized for $z = 2$ and $\nu = 1/2$ and are presented in Figs. 5(c) and 5(d). The value of the critical exponents would seem to indicate that this QPT is in the universality class of free fermions. However, it was argued in [92] that in fact this QPT belongs to the universality class of spin-degenerate impenetrable particle gas with the universal thermodynamics described by Takahashi's formula

[1]It should be noted that the definitions of the chemical potential and effective magnetic field employed by us are different from the ones used in [31], which will be denoted by the $YGZG$ subscript. We have $\mu = \mu_{YGZC}$ and $H = -H_{YGZC}/2$.

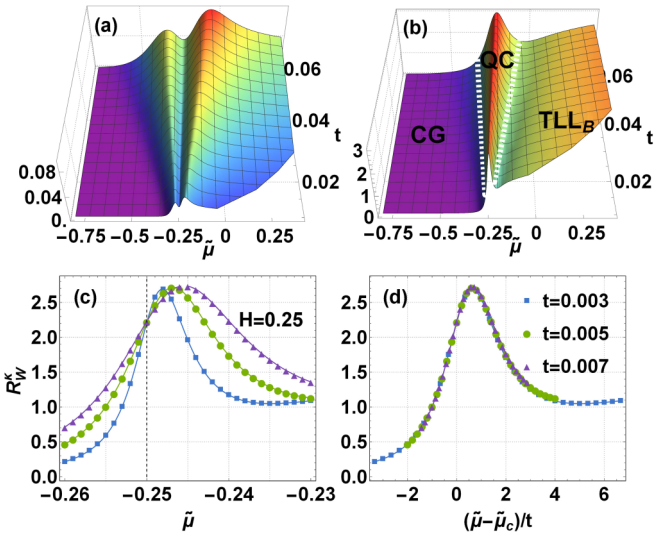

FIG. 5. (a) A 3D plot of the grand-canonical specific heat for $c = 1$ and $H = 0.25$ as a function of the chemical potential and temperature ($\tilde{\mu} = \mu/c^2$ and $t = T/c^2$). The lines of local maxima fanning out from the QCP, $\tilde{\mu}_c = -H/c^2$, are the boundaries of the QC region. (b) A 3D plot of the Wilson ratio. The white dashed lines are the boundaries of the critical region. Here CG represents the vacuum (classical gas) phase and TLL$_B$ is the Tomonaga-Luttinger liquid phase of single-component bosons. (c) Plot of the Wilson ratio as a function of the chemical potential for three values of temperature. All the curves intersect at the QCP (dashed vertical line). The critical exponents are $z = 2$ and $\nu = 1/2$. (d) When plotted as a function of $[\tilde{\mu} - \tilde{\mu}_c(H)]/t$ all the curves collapse to the universal function $\mathcal{Q}_H$ [see Eq. (21)].

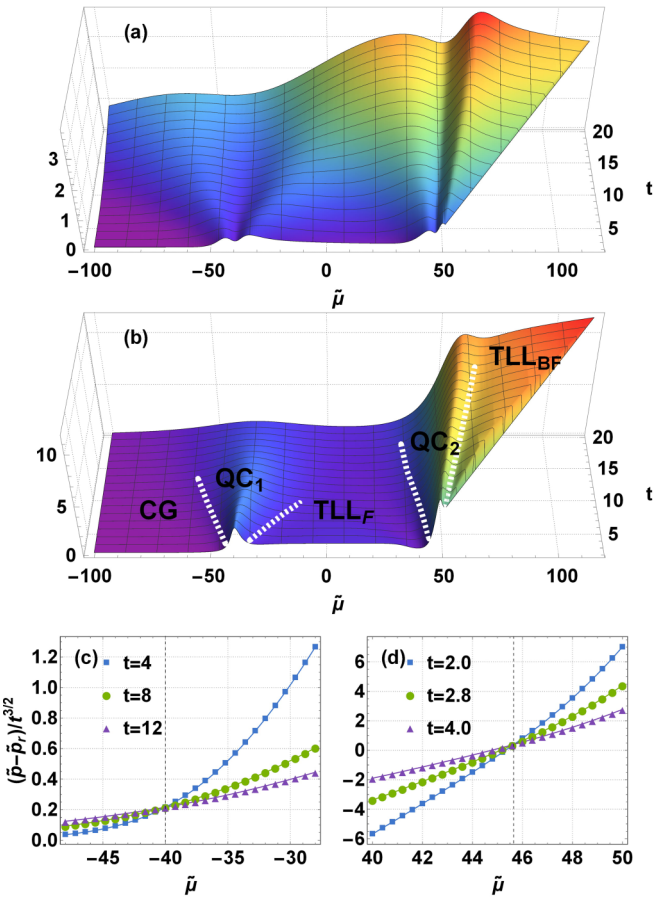

FIG. 6. (a) A 3D plot of the grand-canonical specific heat for $c = 0.05$ and $H = -0.1$ ($\tilde{\mu} = \mu/c^2$ and $t = T/c^2$). In this case we have two sets of lines of local maxima which determine the boundaries of the QC regions emerging from the quantum critical points situated at $\tilde{\mu}_c^{(1)} = -|H|/c^2$ and $\tilde{\mu}_c^{(2)} \sim 0.114/c^2$. (b) A 3D plot of the Wilson ratio. The white dashed lines represent the boundaries of the critical regions QC$_1$ and QC$_2$. Here CG, TLL$_F$, and TLL$_{BF}$ stand for the classical gas phase, the TLL phase of single-component fermions, and the TLL phase of bosons and fermions, respectively. (c) Scaled pressure ($\tilde{p} = p/c^3$) as a function of the chemical potential for three temperatures in the vicinity of the first QCP. For $z = 2$ and $\nu = 1/2$ all the curves intersect at $\tilde{\mu}_c^{(1)} = -|H|/c^2$. (d) Scaled pressure in the vicinity of the second QCP. For $z = 2$ and $\nu = 1/2$ all the curves intersect at $\tilde{\mu}_c^{(2)} \sim 0.114/c^2$.

[66] [$x = (\mu + |H|)/T$ and $y = H/T$]

$$p = \frac{T^{3/2}}{2\pi}\int_{-\infty}^{+\infty} \ln[1 + (1 + e^{-2|y|})e^{-k^2+x}]dk, \qquad (22)$$

in contrast with the free fermionic case for which ($x' = \mu/T$),

$$p_{\rm FF} = \frac{T^{3/2}}{2\pi}\int \ln[(1 + e^{-k^2+x'+y})(1 + e^{-k^2+x'-y})]dk. \qquad (23)$$

In the case of fixed negative magnetic field there are two QPTs. The first QCP is $\mu_c^{(1)} = -|H|$, where the system has a phase transition from the vacuum to a TLL phase of single-component fermions. The value of the second QCP is determined by [$\tilde{\mu}_c^{(2)} = (\mu_c^{(2)} - H)/c^2$] [31]

$$-\frac{2H}{c^2} = \frac{1}{2\pi}\left[\left(1 + 4\tilde{\mu}_c^{(2)}\right)\arctan\left(4\tilde{\mu}_c^{(2)}\right)^{1/2} - \left(4\tilde{\mu}_c^{(2)}\right)^{1/2}\right], \qquad (24)$$

where we have a QPT from the single-component fermionic TLL to a two-component TLL composed of fermions and bosons. The boundaries of the two QC regions for $c = 0.05$ and $H = -0.1$ identified with the maxima of the specific heat are shown in Figs. 6(a) and 6(b). In the case of single-component systems with QPT belonging to the free fermionic universality class, Maeda *et al.* [110] derived a universal relation which determines the boundary between the QC and TLL regions. For $H \gg T$ this relation is also valid for the first QPT of the BFM due to the fact that in this regime Takahashi's formula (22) is equivalent to the pressure of single-component free fermions. We stress that the identification of CR boundaries using the maxima of the specific heat has the advantage of identifying both boundaries in addition to being valid also for multicomponent systems.

The Wilson ratio presents anomalous enhancement in both critical regions. For single-component systems TLL theory predicts that $R_W^\kappa = K$ [106,111], with K the TLL parameter relation which was experimentally verified in the Lieb-Liniger model [106]. This identity is also valid for the Bose-Fermi mixture in the TLL regime of the first QPT for $H \gg T$.

The critical exponents of both QPTs are $z = 2$ and $\nu = 1/2$, as shown in Figs. 6(c) and 6(d), where the curves for the

scaled pressure at different temperatures intersect at $\mu_c^{(1)} = -|H|$ for the first QPT and at $\mu_c^{(2)} = 0.114\,118\ldots$ for the second QPT. While the first transition is in the spin-degenerate universality class characterized by Eq. (22), it is surprising that the second QPT has the same critical exponents as the free fermionic universality class [112]. We point out that the true universal thermodynamics (22) in the vicinity of the critical point $(\mu, H) = (0, 0)$ is different from the free spinor fermion thermodynamics (23). In the case of the first transition, (22) and (23) agree, for $H \gg T$. For the second critical line it is possible that the universal thermodynamics is described by a scaling function different from (22) or (23).

Finally, we like to point out certain similarities of the zero-temperature phase diagram of the Bose-Fermi (BF) system to those of the pure Bose-Bose (BB) and Fermi-Fermi (FF) systems with otherwise the same mass and interaction parameters. For $H \geqslant 0$ the BF phase diagram is identical to that of the BB system with a vacuum phase for $\mu < \mu_c$ and a completely polarized bosonic phase for $\mu > \mu_c$. Viewed from $H > 0$, the line $\mu > 0, H = 0$ is a transition line into a mixed phase. The location of this line is given by the single-particle properties of the new admixed particle; the line does not depend on its statistics.

For $H < 0$ the BF phase diagram is identical to that of the FF system with a vacuum phase for $\mu < \mu_c^{(1)}$, a completely polarized fermionic phase for $\mu_c^{(1)} < \mu < \mu_c^{(2)}$, and a mixed fermionic-bosonic phase for $\mu_c^{(2)} < \mu$. The critical line $\mu_c^{(2)} = \mu_c^{(2)}(H)$ satisfies (24) for the BF and the FF case, as can be derived from the low-temperature limit of the TBA equations for the BF case [31] as well as for the FF case [113]. When approaching this line from the polarized phase, its location is again given by the single-particle properties of the new admixed particle and the line does not depend on its nature.

VI. THE BOSE-FERMI MIXTURE AS THE CONTINUUM LIMIT OF THE PERK-SCHULTZ SPIN CHAIN

The derivation of the BFM's thermodynamic description, (5) and (6), consists of three steps. First, we show that the Perk-Schultz spin chain [114–119] is a lattice embedding of our continuum model. The thermodynamics of the spin chain is then investigated with the quantum transfer-matrix technique [69–74], which relates the free energy of the model to the largest eigenvalue of the QTM and involves only a finite number of NLIEs. Finally, the result for the BFM is obtained by taking the continuum limit in the lattice result. This method was first employed in the case of the Lieb-Liniger model [120] and then used to derive efficient, that is, involving only a finite number of NLIEs, thermodynamic descriptions for the 2CBG [75,76] and the 2CFG [77]. Because the ratios of the largest to the next-largest eigenvalues of the QTM give the correlation lengths of various Green's function, the same algorithm can be used to investigate the asymptotic behavior of correlators in integrable continuum models [121,122].

As in the case of the 2CBG and 2CFG, the lattice embedding of the Bose-Fermi mixture is the critical $q = 3$ Perk-Schultz spin chain [114–119], the only difference being the grading, which in this case is $(-+-)$ (see also [76,77]). Here, by a lattice embedding we understand a lattice model whose spectrum and BAEs transform under a suitable scaling limit in the spectrum and BAEs of the continuum model. The Hamiltonian for an arbitrary grading $(\varepsilon_1, \varepsilon_2, \varepsilon_3)$ $(\varepsilon_i \in \{\pm 1\})$ is

$$\mathcal{H}_{PS} = J\varepsilon_1 \sum_{j=1}^{L} \left(\cos\gamma \sum_{a=1}^{3} \varepsilon_a\, e_{aa}^{(j)} e_{aa}^{(j+1)} + \sum_{\substack{a,b=1 \\ a\neq b}}^{3} e_{ab}^{(j)} e_{ba}^{(j+1)} + i \sin\gamma \sum_{\substack{a,b=1 \\ a\neq b}}^{3} \operatorname{sgn}(a-b) e_{aa}^{(j)} e_{bb}^{(j+1)} \right) - \sum_{j=1}^{L} \sum_{a=1}^{3} h_a e_{aa}^{(j)}, \tag{25}$$

with L the number of lattice sites, $J > 0$ the coupling strength, and h_1, h_2, h_3 chemical potentials. Also, in (25) $\gamma \in [0, \pi]$ is the anisotropy (not to be confused with the dimensionless coupling constant of the continuum model) and $e_{ab}^{(j)} = \mathbb{I}_3^{\otimes j-1} \otimes e_{ab} \otimes \mathbb{I}_3^{\otimes L-j}$, with e_{ab} and $\mathbb{I}_3$ the canonical basis and the unit matrix in the space of 3×3 matrices. For the $(-+-)$ grading the energy spectrum is

$$E_{PS} = \sum_{j=1}^{M} e_0\big(v_j^{(1)}\big) + M_1(h_2 - h_3) + E_0, \quad E_0 = JL\cos\gamma - h_1 L, \quad e_0(v) = \frac{J\sin^2\gamma}{\sin(v-\gamma)\sin v}, \tag{26}$$

with $\{v_s^{(1)}\}_{s=1}^{M}$ and $\{v_l^{(2)}\}_{l=1}^{M_1}$ satisfying the BAEs

$$\left((-1)\frac{\sin\left(v_s^{(1)} - \gamma\right)}{\sin v_s^{(1)}} \right)^L = (-1)^{M-1} \prod_{p=1}^{M_1} \frac{\sin\left(v_s^{(1)} - v_p^{(2)} - \gamma\right)}{\sin\left(v_s^{(1)} - v_p^{(2)}\right)}, \quad s = 1, \ldots, M, \tag{27a}$$

$$\prod_{j=1}^{M} \frac{\sin\left(v_l^{(2)} - v_j^{(1)} + \gamma\right)}{\sin\left(v_l^{(2)} - v_j^{(1)}\right)} = (-1)^{M_1-1}, \quad l = 1, \ldots, M_1. \tag{27b}$$

First, we will show how we can obtain (3) from (27). We consider $v_s^{(1)} \to i\delta k_s^{(1)}/\epsilon + \gamma/2$ and $v_s^{(2)} \to i\delta k_s^{(2)}/\epsilon + \pi/2$ with $\epsilon \to 0$ and lattice constant $\delta \to O(\epsilon^2)$. Under this transformation Eqs. (27) become

$$\left((-1)\frac{\sinh\left(\delta k_s^{(1)}/\epsilon - i\gamma/2\right)}{\sinh\left(\delta k_s^{(1)}/\epsilon + i\gamma/2\right)}\right)^L = (-1)^{M-1}\prod_{p=1}^{M_1}\frac{\cosh\left(\delta k_s^{(1)}/\epsilon - \delta k_p^{(2)}/\epsilon - i\gamma/2\right)}{\cosh\left(\delta k_s^{(1)}/\epsilon - \delta k_p^{(2)}/\epsilon + i\gamma/2\right)}, \quad s = 1,\ldots,M,$$

$$\prod_{j=1}^{M}\frac{\cosh\left(\delta k_l^{(2)}/\epsilon - \delta k_j^{(1)}/\epsilon - i\gamma/2\right)}{\cosh\left(\delta k_l^{(2)}/\epsilon - \delta k_j^{(1)}/\epsilon + i\gamma/2\right)} = (-1)^{M_1-1}, \quad l = 1,\ldots,M_1.$$

In the second step we perform $\gamma \to \pi - \epsilon$, with the result

$$\left(\frac{\cosh\left(\delta k_s^{(1)} + i\epsilon/2\right)}{\cosh\left(\delta k_s^{(1)} - i\epsilon/2\right)}\right)^L = (-1)^{M+M_1-1}\prod_{p=1}^{M_1}\frac{\sinh\left(\delta k_s^{(1)}/\epsilon - \delta k_p^{(2)}/\epsilon + i\epsilon/2\right)}{\sinh\left(\delta k_s^{(1)}/\epsilon - \delta k_p^{(2)}/\epsilon - i\epsilon/2\right)}, \quad s = 1,\ldots,M, \tag{28a}$$

$$\prod_{j=1}^{M}\frac{\sinh\left(\delta k_l^{(2)}/\epsilon - \delta k_j^{(1)}/\epsilon + i\epsilon/2\right)}{\sinh\left(\delta k_l^{(2)}/\epsilon - \delta k_j^{(1)}/\epsilon - i\epsilon/2\right)} = (-1)^{M+M_1-1}, \quad l = 1,\ldots,M_1. \tag{28b}$$

Taking the limit $L \to \infty$ such that $L\delta = L_{BF}$, introducing $c = \epsilon^2/\delta$, and using

$$\frac{\cosh\left(\delta k_s^{(1)} + i\epsilon/2\right)}{\cosh\left(\delta k_s^{(1)} - i\epsilon/2\right)} \sim \frac{1 + i\delta k_s^{(1)}/2}{1 - i\delta k_s^{(1)}/2},$$

we see that Eqs. (28) transform into the BAEs of the mixture (3) for $M_1 + M - 1$ even and identifying $M_1 = M_B$. Under the same set of transformations we have

$$E_{PS} - E_0 = \sum_{j=1}^{M}\left[J\delta^2\left(k_j^{(1)}\right)^2 - J\epsilon^2 - J\epsilon^4/4 + h_1 - h_2\right] + (h_2 - h_3)M_1 + O(\epsilon^6).$$

However, we are interested in the thermodynamic behavior and therefore we can also scale the temperature in the models in order to have $\beta(E_{PS} - E_0) \to \bar{\beta}E_{BF}$, with E_{BF} given by (2). If we consider $J = 1$, $\beta = \bar{\beta}/\delta^2$, $h_1 \to O(\epsilon^2)$ such that $(J\epsilon^2 - h_1)/\delta^2$ is finite, and $h_2, h_3 \to O(\epsilon^4)$, we obtain $\beta(E_{PS} - E_0) \to \bar{\beta}E_{BF}$, with $\mu_F = J\epsilon^2 + J\epsilon^4/4 - h_1 + h_2)/\delta^2$ and $\mu_B - \mu_F = (h_3 - h_2)/\delta^2$. The scaling limit presented in this section is the same as the one used in the 2CBG and 2CFG cases (see Table I of [76]) and shows that the thermodynamic behavior of the mixture at all temperatures can be derived from the low-temperature thermodynamics of the lattice model.

VII. DERIVATION OF THE THERMODYNAMICS FOR THE PERK-SCHULTZ SPIN CHAIN

The free energy of the Perk-Schultz spin chain can be obtained from the largest eigenvalue of the QTM as $f(h_1, h_2, h_3, \beta) = -\ln\Lambda_0(0)/\beta$. For a given Trotter number, denoted by N, the largest eigenvalue of the QTM lies in the $(N/2, N/2)$ sector (see Appendix A of [76] or [124–127]) and can be written as

$$\Lambda_0(v) = \lambda_1(v) + \lambda_2(v) + \lambda_3(v), \tag{29}$$

with

$$\lambda_j(v) = \phi_-(v)\phi_+(v)\frac{q_{j-1}(v - i\tilde{\epsilon}_j\gamma)}{q_{j-1}(v)}\frac{q_j(v + i\tilde{\epsilon}_j\gamma)}{q_j(v)}e^{\beta\tilde{h}_j}, \tag{30}$$

where $(\tilde{\epsilon}_1, \tilde{\epsilon}_2, \tilde{\epsilon}_3) = (- - +)$, $(\tilde{h}_1, \tilde{h}_2, \tilde{h}_3) = (h_3, h_1, h_2)$, and

$$\phi_\pm(v) = \left(\frac{\sinh(v \pm iu)}{\sin\gamma}\right)^{N/2}, \quad u = J\sin\gamma\beta/N. \tag{31}$$

The $q_j(v)$ functions are defined as

$$q_j(v) = \begin{cases}\phi_-(v), & j = 0\\ \prod_{k=1}^{N/2}\sinh\left(v - v_k^{(j)}\right), & j = 1, 2\\ \phi_+(v), & j = 3,\end{cases} \tag{32}$$

with $\{v_k^{(1)}\}_{k=1}^{N/2}$ and $\{v_k^{(2)}\}_{k=1}^{N/2}$ parameters which are called Bethe roots and satisfy the quantum transfer-matrix BAEs (discussed below). If we introduce two auxiliary functions

$$\mathfrak{a}_1 = \frac{\lambda_1(v)}{\lambda_2(v)} = \frac{\phi_-(v + i\gamma)}{\phi_-(v)}\frac{q_1(v - i\gamma)}{q_1(v + i\gamma)}\frac{q_2(v)}{q_2(v - i\gamma)}e^{\beta(h_3 - h_1)}, \tag{33a}$$

$$\mathfrak{a}_2 = \frac{\lambda_3(v)}{\lambda_2(v)} = \frac{\phi_+(v + i\gamma)}{\phi_+(v)}\frac{q_1(v)}{q_1(v + i\gamma)}e^{\beta(h_2 - h_1)}, \tag{33b}$$

the BAEs of the quantum transfer matrix can be written as $(j = 1, 2)$ $\mathfrak{a}_j(v_k^{(j)}) = -1$, $k = 1,\ldots,N/2$.

A. Integral equations for the auxiliary functions

First, we will derive a set of NLIEs for the auxiliary functions (33). Both of the functions are periodic of period $i\pi$. The equation $\mathfrak{a}_1(v) = -1$ has $3N/2$ solutions, of which $N/2$ are the so-called Bethe roots $\{v_j^{(1)}\}_{j=1}^{N/2}$, and N solutions, which are called holes and are denoted by $\{v'^{(1)}_j\}_{j=1}^{N}$. However, the second equation $\mathfrak{a}_2(v) = -1$ has only N solutions, of which $N/2$ are the Bethe roots $\{v_j^{(2)}\}_{j=1}^{N}$ and the other $N/2$ are the second set of holes denoted by $\{v'^{(2)}_j\}_{j=1}^{N/2}$. A typical distribution of Bethe roots and holes characterizing the largest

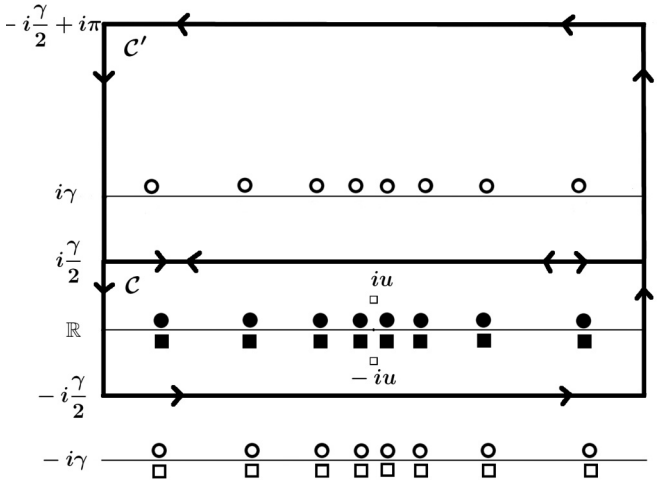

FIG. 7. Distribution of Bethe roots (■ and ●) and holes (□ and ○) for the largest eigenvalue of the QTM and $\gamma \in (0, \pi/2)$. The contour $\mathcal{C}$ contains all the Bethe roots and the poles of order $N/2$ at $\pm iu$. The lower edge of the contour $\mathcal{C}'$ coincides with the upper edge of $\mathcal{C}$ but it has opposite orientation.

eigenvalue of the QTM for $\gamma \in (0, \pi/2)$ is shown in Fig. 7. For any value of the Trotter number N the strip $|\mathrm{Im} v| < \gamma/2$ contains all the Bethe roots and the poles of order $N/2$ at $\pm iu$. Introducing the rectangular contour $\mathcal{C}$ centered at the origin, which extends to infinity and is depicted in Fig. 7, we can define for v outside of $\mathcal{C}$ ($j = 1, 2$),

$$f_j(v) = \frac{1}{2\pi i}\int_{\mathcal{C}} \frac{d}{dv}[\ln\sinh(v-w)]\ln[1+\mathfrak{a}_j(w)]dw$$
$$= \frac{1}{2\pi i}\int_{\mathcal{C}} \ln\sinh(v-w)\frac{\mathfrak{a}_j'(w)}{1+\mathfrak{a}_j(w)}dw. \tag{34}$$

The last relation was derived using integration by parts and the fact that the winding number of $\ln[1+\mathfrak{a}_j(w)]$ is zero due to the fact that the number of zeros and order of the poles inside the contour are the same. Then we can show that (see [123] or [76,77])

$$f_1(v) = \ln q_1(v) - \ln\phi_-(v) - \frac{N}{2}\ln\sin\gamma, \tag{35a}$$

$$f_1(v) = \ln q_2(v) - \ln\phi_+(v) - \frac{N}{2}\ln\sin\gamma. \tag{35b}$$

Taking the logarithm of the auxiliary functions (33) and using the previous result (35), we obtain

$$\ln\mathfrak{a}_1(v) = \beta(h_3-h_1) + \ln\left[\frac{\phi_+(v)}{\phi_-(v)}\frac{\phi_-(v-i\gamma)}{\phi_+(v-i\gamma)}\right]$$
$$+ f_1(v-i\gamma) - f_1(v+i\gamma) + f_2(v) - f_2(v-i\gamma),$$
$$\ln\mathfrak{a}_2(v) = \beta(h_2-h_1) + \ln\left[\frac{\phi_-(v)}{\phi_+(v)}\frac{\phi_+(v+i\gamma)}{\phi_-(v+i\gamma)}\right]$$
$$+ f_1(v) - f_1(v+i\gamma).$$

Now we can take the Trotter limit $\lim_{N\to\infty} \ln[\phi_+(v)/\phi_-(v)] = iJ\beta\sin\gamma\coth v$, with the result

$$\ln\mathfrak{a}_1(v) = \beta(h_3-h_1) - \beta\frac{J\sinh^2 i\gamma}{\sinh v\sinh(v-i\gamma)}$$
$$+\int_{\mathcal{C}}\bar{K}_0(v-w)\ln[1+\mathfrak{a}_1(w)]dw$$
$$-\int_{\mathcal{C}}\bar{K}_2(v-w)\ln[1+\mathfrak{a}_2(w)]dw, \tag{37a}$$
$$\ln\mathfrak{a}_2(v) = \beta(h_2-h_1) - \beta\frac{J\sinh^2 i\gamma}{\sinh v\sinh(v+i\gamma)}$$
$$+\int_{\mathcal{C}}\bar{K}_1(v-w)\ln[1+\mathfrak{a}_1(w)]dw, \tag{37b}$$

where

$$\bar{K}_0(v) = \frac{1}{2\pi i}\frac{\sinh 2i\gamma}{\sinh(v+i\gamma)\sinh(v-i\gamma)}, \tag{38}$$
$$\bar{K}_1(v) = \frac{1}{2\pi i}\frac{\sinh i\gamma}{\sinh(v)\sinh(v+i\gamma)}, \tag{39}$$
$$\bar{K}_2(v) = \frac{1}{2\pi i}\frac{\sinh i\gamma}{\sinh(v)\sinh(v-i\gamma)}. \tag{40}$$

Equations (37) were derived assuming $\gamma \in (0, \pi/2)$ and v is outside the contour. For v inside the contour we need to add a $\ln[1+\mathfrak{a}_2(v)]$ term on the right-hand side of Eq. (37a) and a $\ln[1+\mathfrak{a}_1(v)]$ term on the right-hand side of Eq. (37b). For $\gamma \in (\pi/2, \pi)$ the same equations remain valid if we replace $\mathcal{C}$ with a similar rectangular contour with horizontal edges situated at $\pm i(\pi-\gamma-\epsilon)/2$.

B. Integral expression for the largest eigenvalue

The largest eigenvalue of the QTM is analytic in a strip around the real axis, therefore it will be sufficient to derive an integral expression for $\ln\Lambda_0(v_0)$ with v_0 close to the real axis and then take the limit $v_0 \to 0$ to obtain the free energy. For our purposes we choose $v_0 = iu$, for which $\lambda_3(v_0) = 0$ and (c is a constant)

$$\Lambda_0(v_0) = \lambda_1(v_0) + \lambda_2(v_0) = c\frac{\phi_+(v_0)q_1^{(h)}(v_0)}{q_2(v_0)}, \tag{41}$$

where we have used the identity (A1) and $q_i^{(h)}(v)$ are defined in the Appendix.

Consider v inside the contour $\mathcal{C}$. Then, inside the contour $\mathcal{C}'$ depicted in Fig. 7, the function $1+\mathfrak{a}_1(v)$ has N zeros identified with the holes $\{v_j'^{(1)}\}_{j=1}^N$, $N/2$ poles located at $\{v_j^{(1)} - i\gamma\}_{j=1}^{N/2}$, and $N/2$ poles located at $\{v_j^{(2)} + i\gamma\}_{j=1}^{N/2}$ (some of the holes and poles are modulo $i\pi$). This means that around $\mathcal{C}'$ the function $\ln[1+\mathfrak{a}_1(v)]$ has zero winding number. Using the identity (A6) in the form [$d(v) = d\ln\sinh v/dv$]

$$\int_{\mathcal{C}} d(v-w)\frac{\mathfrak{a}_j'(w)}{1+\mathfrak{a}_j(w)}dw = -\int_{\mathcal{C}'} d(v-w)\frac{\mathfrak{a}_j'(w)}{1+\mathfrak{a}_j(w)}dw,$$

the right-hand side can be computed as (35), with the result

$$\frac{1}{2\pi i}\int_{\mathcal{C}} d(v-w)\frac{\mathfrak{a}_1'(w)}{1+\mathfrak{a}_1(w)}dw = \sum_{j=1}^{N/2} d\big(v-v_j^{(1)}+i\gamma\big)+\sum_{j=1}^{N/2} d\big(v-v_j^{(2)}-i\gamma\big)-\sum_{j=1}^{N} d\big(v-v_j'^{(1)}\big). \tag{42}$$

After integration by parts with respect to w and then integration with respect to v we find

$$\frac{1}{2\pi i}\int_{\mathcal{C}} d(v-w)\ln[1+\mathfrak{a}_1(w)]dw = -\ln q_1^{(h)}(v)+\ln q_1(v+i\gamma)+\ln q_2(v-i\gamma)+c. \tag{43}$$

In a similar fashion, using the fact that inside $\mathcal{C}'$ the function $1+\mathfrak{a}_2(v)$ has $N/2$ zeros at the holes $\{v_j'^{(2)}\}_{j=1}^{N/2}$ and $N/2$ poles located at$\{v_j^{(1)}-i\gamma\}_{j=1}^{N/2}$ (some modulo $i\pi$), we find

$$\frac{1}{2\pi i}\int_{\mathcal{C}} d(v-w)\ln[1+\mathfrak{a}_2(w)]dw = -\ln q_2^{(h)}(v)+\ln q_1(v+i\gamma)+c. \tag{44}$$

For v inside $\mathcal{C}$, $v\pm i\gamma$ is outside of the contour. Therefore, from (35) we have

$$\frac{1}{2\pi i}\int_{\mathcal{C}} d(v-w)\ln[1+\mathfrak{a}_1(w)]dw = \ln q_1(v+i\gamma)-\ln\phi_-(v+i\gamma)-\frac{N}{2}\sin\gamma, \tag{45a}$$

$$\frac{1}{2\pi i}\int_{\mathcal{C}} d(v-w)\ln[1+\mathfrak{a}_2(w)]dw = \ln q_2(v-i\gamma)-\ln\phi_+(v-i\gamma)-\frac{N}{2}\sin\gamma. \tag{45b}$$

Subtracting Eq. (43) from Eq. (45a) and Eq. (44) from Eq. (45b), we obtain

$$\int_{\mathcal{C}} \bar{K}_1(v-w)\ln[1+\mathfrak{a}_1(w)]dw = -\ln q_1^{(h)}(v)+\ln q_2(v-i\gamma)+\ln\phi_-(v+i\gamma)+c, \tag{46a}$$

$$-\int_{\mathcal{C}} \bar{K}_2(v-w)\ln[1+\mathfrak{a}_2(w)]dw = -\ln q_2^{(h)}(v)+\ln q_1(v+i\gamma)-\ln q_2(v-i\gamma)+\ln\phi_+(v-i\gamma)+c. \tag{46b}$$

The importance of this result becomes apparent by noticing that the expression of the largest eigenvalue (41) can be rewritten using (A5) as

$$\ln\Lambda_0(v_0) = \ln q_1^{(h)}(v_0)+\ln q_2^{(h)}(v_0)-\ln q_1(v_0+i\gamma)-\ln[1+\mathfrak{a}_2(v_0)]+c$$

and then using (46) as

$$\begin{aligned}\ln\Lambda_0(v_0) = &-\int_{\mathcal{C}}\bar{K}_1(v_0-w)\ln[1+\mathfrak{a}_1(w)]dw+\int_{\mathcal{C}}\bar{K}_2(v_0-w)\ln[1+\mathfrak{a}_2(w)]dw\\ &-\ln[1+\mathfrak{a}_2(v_0)]+\ln[\phi_+(v_0-i\gamma)\phi_-(v_0+i\gamma)]+c.\end{aligned} \tag{47}$$

The constant of integration can be computed by noticing that Eq. (47) is in fact valid for all v in a narrow strip around the real axis with $\ln[\lambda_1(v)+\lambda_2(v)]$ replacing the left-hand side. Considering the limit $v\to\infty$ and using $\lim_{v\to\infty}[\lambda_1(v)+\lambda_2(v)]/\phi_+(v-i\gamma)\phi_-(v+i\gamma) = e^{\beta h_1}+e^{\beta h_3}$, we find

$$c = \beta h_1 + c', \tag{48}$$

with $c' = 2\ln[(1+e^{\beta(h_3-h_1)})(1+e^{\beta(h_2-h_1)})]$. Finally, by taking the Trotter limit $N\to\infty$ and using $\lim_{N\to\infty}\ln[\phi_+(v_0-i\gamma)\phi_-(v_0+i\gamma)] = -J\cos\gamma\beta$, we obtain

$$\ln\Lambda_0(0) = c - J\beta\cos\gamma - \int_{\mathcal{C}}\bar{K}_2(w)\ln[1+\mathfrak{a}_1(w)]dw+\int_{\mathcal{C}}\bar{K}_1(w)\ln[1+\mathfrak{a}_2(w)]dw-\ln[1+\mathfrak{a}_2(0)]. \tag{49}$$

This result was derived for $\gamma\in(0,\pi/2)$, but it remains valid also for $\gamma\in(\pi/2,\pi)$ if $\mathcal{C}$ is replaced by a rectangular contour with the horizontal edges situated at $\pm i(\pi-\gamma-\epsilon)/2$.

C. Continuum limit

The continuum limit (see Sec. VI) of the integral equations (37) and integral expression for the largest eigenvalue (49) is the same as the one performed for the 2CBG and is presented in detail in [76]. In the scaling limit we obtain Eq. (5) for the grand-canonical potential of the continuum model with the auxiliary functions satisfying the NLIEs (6).

VIII. CONCLUSION

In this paper we have derived an alternative thermodynamic description for the Bose-Fermi mixture in the QTM framework and performed a detailed analysis of the contact at

zero and finite temperatures. In the strong-coupling regime the contact develops a pronounced local minimum as a function of the temperature which is accompanied by a significant momentum reconstruction at both low and large momenta. This momentum reconstruction can be experimentally detected and provides an identification of the transition from the TLL to the spin-incoherent regime. In addition, we have also shown that the boundaries of the QC regions can be well mapped by the maxima of the grand-canonical specific heat. Our results also hint at the possibility of deriving efficient thermodynamic descriptions for integrable κ component ($\kappa > 2$), systems with contact interactions involving only κ integral equations.

ACKNOWLEDGMENTS

O.I.P. acknowledges financial support from the LAPLAS 4 and 5 programs of the Romanian National Authority for Scientific Research (CNCS-UEFISCDI). Both authors are grateful to Deutsche Forschungsgemeinschaft for support via Research Unit FOR 2316.

APPENDIX: SOME USEFUL IDENTITIES

In this Appendix we prove certain identities which are needed in the derivation of the integral expression of the largest QTM eigenvalue. First, we will prove that

$$\lambda_1(v) + \lambda_2(v) = c\frac{\phi_+(v)q_1^{(h)}(v)}{q_2(v)}, \tag{A1}$$

with c a constant and $q_1^{(h)}(v)$ defined by

$$q_1^{(h)} = \prod_{i=1}^{N} \sinh\left(v - v_i'^{(1)}\right). \tag{A2}$$

From the definition of the $\lambda_j(v)$ functions we obtain

$$\lambda_1(v) + \lambda_2(v) = \frac{\phi_+(v)p_1(v)}{q_1(v)q_2(v)},$$

with $p_1(v) = [\phi_-(v+i\gamma)q_1(v-i\gamma)q_2(v)e^{\beta h_3} + \phi_-(v)q_1(v+i\gamma)q_2(v-i\gamma)e^{\beta h_1}$. The equation $p_1(v) = 0$ [which is equivalent to $\mathfrak{a}_1(v) = -1$] has $3N/2$ solutions which are the $N/2$ Bethe roots $\{v_j^{(1)}\}_{j=1}^{N/2}$ and the N holes $\{v_j'^{(1)}\}_{j=1}^{N}$. Also $p_1(v+i\pi) = (-1)^{3N/2}p(v)$ and $\lim_{v\to\infty} p_1(v)/\sinh^{3N/2} v = \text{const}$, which shows that $p_1(v) = c\,q_1(v)q_1^{(h)}(v)$. This concludes the proof of (A1).

A similar identity is

$$\lambda_2(v) + \lambda_3(v) = c\frac{\phi_-(v)q_2(v-i\gamma)q_2^{(h)}(v)}{q_1(v)}, \tag{A3}$$

with

$$q_2^{(h)} = \prod_{i=1}^{N/2} \sinh\left(v - v_i'^{(2)}\right). \tag{A4}$$

Again, from the definition we have

$$\lambda_2(v) + \lambda_3(v) = \frac{\phi_-(v)q_2(v-i\gamma)p_2(v)}{q_1(v)q_2(v)},$$

with $p_2(v) = [\phi_+(v)q_1(v+i\gamma)e^{\beta h_1} + q_1(v)\phi_+(v+i\gamma)e^{\beta h_2}]$. The equation $p_2(v) = 0$ [equivalent to $\mathfrak{a}_2(v) = -1$] has N solutions which are the $N/2$ Bethe roots $\{v_j^{(2)}\}_{j=1}^{N/2}$ and the $N/2$ holes $\{v_j'^{(2)}\}_{j=1}^{N/2}$. In addition, we have $p_2(v+i\pi) = (-1)^N p_2(v)$ and $\lim_{v\to\infty} p_2(v)/\sinh^N v = \text{const}$, which shows that $p_2(v)$ can be written as $p_2(v) = cq_2(v)q_2^{(h)}(v)$, concluding the proof of (A3). Also, we have $\ln[1+\mathfrak{a}_2(v)] = \ln[p_2(v)/\phi_+(v)q_1(v+i\gamma)]$, which is equivalent to

$$\begin{aligned} &-\ln\phi_+(v) + \ln q_2(v) - \ln q_1(v+i\gamma) \\ &\quad + \ln q_2^{(h)}(v) - \ln[1+\mathfrak{a}_2(v)] + \text{const} = 0. \end{aligned} \tag{A5}$$

In Sec. VII B we will also use [$d(v) = \frac{d}{dv}\ln\sinh v$]

$$\int_{\mathcal{C}+\mathcal{C}'} d(v-w)\frac{\mathfrak{a}_j'(w)}{1+\mathfrak{a}_j(w)}dw = 0, \tag{A6}$$

with the contours depicted in Fig. 7. The proof is similar to the one described in [76,77] for the 2CBG and 2CFG cases and is left to the reader.

[1] I. Bloch, J. Dalibard, and W. Zwerger, Many-body physics with ultracold gases, Rev. Mod. Phys. **80**, 885 (2008).
[2] M. A. Cazalilla, R. Citro, T. Giamarchi, E. Orignac, and M. Rigol, One dimensional bosons: From condensed matter systems to ultracold gases, Rev. Mod. Phys. **83**, 1405 (2011).
[3] X.-W. Guan, M. T. Batchelor, and C. Lee, Fermi gases in one dimension: From Bethe ansatz to experiments, Rev. Mod. Phys. **85**, 1633 (2013).
[4] R. Onofrio, Cooling and thermometry of atomic Fermi gases, Phys. Usp. **59**, 1129 (2016).
[5] K. K. Das, Bose-Fermi Mixtures in One Dimension, Phys. Rev. Lett. **90**, 170403 (2003).
[6] Z. Akdeniz, P. Vignolo, and M. P. Tosi, Boson-fermion mixtures inside an elongated cigar-shaped trap, J. Phys. B **38**, 2933 (2005).
[7] F. M. Marchetti, T. Jolicoeur, and M. M. Parish, Stability and Pairing in Quasi-One-Dimensional Bose-Fermi Mixtures, Phys. Rev. Lett. **103**, 105304 (2009).
[8] D. Rakshit, T. Karpiuk, M. Brewczyk, M. Lewenstein, and M. Gajda, Self-bound Bose-Fermi liquids in lower dimensions, arXiv:1808.04793.
[9] M. A. Cazalilla and A. F. Ho, Instabilities in Binary Mixtures of One-Dimensional Quantum Degenerate Gases, Phys. Rev. Lett. **91**, 150403 (2003).
[10] L. Mathey, D.-W. Wang, W. Hofstetter, M. D. Lukin, and E. Demler, Luttinger Liquid of Polarons in One-Dimensional Boson-Fermion Mixtures, Phys. Rev. Lett. **93**, 120404 (2004).
[11] H. Frahm and G. Palacios, Correlation functions of one-dimensional Bose-Fermi mixtures, Phys. Rev. A **72**, 061604(R) (2005).

[12] L. Mathey and D.-W. Wang, Phase diagrams of one-dimensional Bose-Fermi mixtures of ultracold atoms, Phys. Rev. A **75**, 013612 (2007).

[13] E. Orignac, M. Tsuchiizu, and Y. Suzumura, Competition of superfluidity and density waves in one-dimensional Bose-Fermi mixtures, Phys. Rev. A **81**, 053626 (2010).

[14] B. Reichert, A. Petković, and Z. Ristivojevic, Quasiparticle decay in a one-dimensional Bose-Fermi mixture, Phys. Rev. B **95**, 045426 (2017).

[15] P. Schlottmann, Threshold singularities in the one-dimensional supersymmetric boson-fermion gas mixture, Int. J. Mod. Phys. B **32**, 1850221 (2018).

[16] T. Miyakawa, H. Yabu, and T. Suzuki, Peierls instability, periodic Bose-Einstein condensates, and density waves in quasi-one-dimensional boson-fermion mixtures of atomic gases, Phys. Rev. A **70**, 013612 (2004).

[17] E. Nakano and H. Yabu, Density waves in a quasi-one-dimensional atomic gas mixture of bosons and two-component fermions, Phys. Rev. A **72**, 043602 (2005).

[18] C. K. Lai and C. N. Yang, Ground-state energy of a mixture of fermions and bosons in one dimension with a repulsive δ-function interaction, Phys. Rev. A **3**, 393 (1971).

[19] C. K. Lai, Thermodynamics of Fermions in One Dimension with a δ-Function Interaction, Phys. Rev. Lett. **26**, 1472 (1971).

[20] C. K. Lai, Thermodynamics of a mixture of fermions and bosons in one dimension with a repulsive δ-function potential, J. Math. Phys. **15**, 954 (1974).

[21] M. T. Batchelor, M. Bortz, X.-W. Guan, and N. Oelkers, Exact results for the one-dimensional mixed boson-fermion interacting gas, Phys. Rev. A **72**, 061603(R) (2005).

[22] N. Oelkers, M. T. Batchelor, M. Bortz, and X. W. Guan, Bethe ansatz study of one-dimensional Bose and Fermi gases with periodic and hard wall boundary conditions, J. Phys. A: Math. Gen. **39**, 1073 (2006).

[23] X.-W. Guan, M. T. Batchelor, and J.-Y. Lee, Magnetic ordering and quantum statistical effects in strongly repulsive Fermi-Fermi and Bose-Fermi mixtures, Phys. Rev. A **78**, 023621 (2008).

[24] A. Imambekov and E. Demler, Exactly solvable case of a one-dimensional Bose-Fermi mixture, Phys. Rev. A **73**, 021602(R) (2006).

[25] A. Imambekov and E. Demler, Applications of exact solution for strongly interacting one-dimensional Bose-Fermi mixture: Low-temperature correlation functions, density profiles, and collective modes, Ann. Phys. (NY) **321**, 2390 (2006).

[26] Z.-X. Hu, Q.-L. Zhang, and Y.-Q. LiGround state properties of one-dimensional Bose-Fermi mixtures, J. Phys. A: Math. Gen. **39**, 351 (2006).

[27] X. Yin, S. Chen, and Y. Zhang, Yang-Yang thermodynamics of a Bose-Fermi mixture, Phys. Rev. A **79**, 053604 (2009).

[28] S.-J. Gu, J. Cao, S. Chen, and H.-Q. Lin, Quantum phase transition and elementary excitations of a Bose-Fermi mixture in a one-dimensional optical lattice, Phys. Rev. B **80**, 224508 (2009).

[29] Y.-J. Hao, Ground state density distribution of Bose-Fermi mixture in a one-dimensional harmonic trap, Chin. Phys. Lett. **28**, 010302 (2011).

[30] Y.-J. Hao, Composite-fermionization of the mixture composed of Tonks gas and Fermi gas, Chin. Phys. B **20**, 060307 (2011).

[31] X. Yin, X.-W. Guan, Y. Zhang, and S. Chen, Quantum criticality of a one-dimensional Bose-Fermi mixture, Phys. Rev. A **85**, 013608 (2012).

[32] P. Schlottmann, Mixture of interacting supersymmetric spinless fermions and bosons in a one-dimensional trap, Mod. Phys. Lett. B **30**, 1630007 (2016).

[33] Y. Takeuchi and H. Mori, Mixing-demixing transition in one-dimensional boson-fermion mixtures, Phys. Rev. A **72**, 063617 (2005).

[34] L. Pollet, M. Troyer, K. Van Houcke, and S. M. A. Rombouts, Phase Diagram of Bose-Fermi Mixtures in One-Dimensional Optical Lattices, Phys. Rev. Lett. **96**, 190402 (2006).

[35] P. Sengupta and L. P. Pryadko, Quantum degenerate Bose-Fermi mixtures on one-dimensional optical lattices, Phys. Rev. B **75**, 132507 (2007).

[36] A. Mering and M. Fleischhauer, One-dimensional Bose-Fermi-Hubbard model in the heavy-fermion limit, Phys. Rev. A **77**, 023601 (2008).

[37] A. Zujev, A. Baldwin, R. T. Scalettar, V. G. Rousseau, P. J. H. Denteneer, and M. Rigol, Superfluid and Mott-insulator phases of one-dimensional Bose-Fermi mixtures, Phys. Rev. A **78**, 033619 (2008).

[38] X. Barillier-Pertuisel, S. Pittel, L. Pollet, and P. Schuck, Boson-fermion pairing in Bose-Fermi mixtures on one-dimensional optical lattices, Phys. Rev. A **77**, 012115 (2008).

[39] M. Rizzi and A. Imambekov, Pairing of one-dimensional Bose-Fermi mixtures with unequal masses, Phys. Rev. A **77**, 023621 (2008).

[40] H. Wang, Y. Hao, and Y. Zhang, Density-functional theory for one-dimensional harmonically trapped Bose-Fermi mixture, Phys. Rev. A **85**, 053630 (2012).

[41] K. K. Nielsen, Z. Wu, and G. M. Bruun, Higher first Chern numbers in one-dimensional Bose–Fermi mixtures, New J. Phys. **20**, 025005 (2018).

[42] M. D. Girardeau and A. Minguzzi, Soluble Models of Strongly Interacting Ultracold Gas Mixtures in Tight Waveguides, Phys. Rev. Lett. **99**, 230402 (2007).

[43] B. Fang, P. Vignolo, C. Miniatura, and A. Minguzzi, Fermionization of a strongly interacting Bose-Fermi mixture in a one-dimensional harmonic trap, Phys. Rev. A **79**, 023623 (2009).

[44] B. Fang, P. Vignolo, M. Gattobigio, C. Miniatura, and A. Minguzzi, Exact solution for the degenerate ground-state manifold of a strongly interacting one-dimensional Bose-Fermi mixture, Phys. Rev. A **84**, 023626 (2011).

[45] J. Decamp, J. Jünemann, M. Albert, M. Rizzi, A. Minguzzi, and P. Vignolo, High-momentum tails as magnetic structure probes for strongly correlated SU(κ) fermionic mixtures in one-dimensional traps, Phys. Rev. A **94**, 053614 (2016).

[46] J. Decamp, J. Jünemann, M. Albert, M. Rizzi, A. Minguzzi, and P. Vignolo, Strongly correlated one-dimensional Bose-Fermi quantum mixtures: Symmetry and correlations, New J. Phys. **19**, 125001 (2017).

[47] J. Decamp, P. Armagnat, B. Fang, M. Albert, A. Minguzzi, and P. Vignolo, Exact density profiles and symmetry classification for strongly interacting multicomponent Fermi gases in tight waveguides, New J. Phys. **18**, 055011 (2016).

[48] K. Lelas, D. Jukić, and H. Buljan, Ground-state properties of a one-dimensional strongly interacting Bose-Fermi mixture in a double-well potential, Phys. Rev. A **80**, 053617 (2009).

[49] X. Lü, X. Yin, and Y. Zhang, Hard-core Bose-Fermi mixture in one-dimensional split traps, Phys. Rev. A **81**, 043607 (2010).

[50] S. Chen, J. Cao, and S.-J. Gu, Mixture of Tonks-Girardeau gas and Fermi gas in one-dimensional optical lattices, Phys. Rev. A **82**, 053625 (2010).

[51] H. Hu, L. Guan, and S. Chen, Strongly interacting Bose-Fermi mixtures in one dimension, New J. Phys. **18**, 025009 (2016).

[52] F. Deuretzbacher, D. Becker, J. Bjerlin, S. M. Reimann, and L. Santos, Spin-chain model for strongly interacting one-dimensional Bose-Fermi mixtures, Phys. Rev. A **95**, 043630 (2017).

[53] F. Deuretzbacher, K. Fredenhagen, D. Becker, K. Bongs, K. Sengstock, and D. Pfannkuche, Exact Solution of Strongly Interacting Quasi-One-Dimensional Spinor Bose Gases, Phys. Rev. Lett. **100**, 160405 (2008).

[54] F. Deuretzbacher, D. Becker, J. Bjerlin, S. M. Reimann, and L. Santos, Quantum magnetism without lattices in strongly interacting one-dimensional spinor gases, Phys. Rev. A **90**, 013611 (2014).

[55] A. G. Volosniev, D. V. Fedorov, A. S. Jensen, M. Valiente, and N. T. Zinner, Strongly interacting confined quantum systems in one dimension, Nat. Commun. **5**, 5300 (2014).

[56] N. J. S. Loft, L. B. Kristensen, A. E. Thomsen, and N. T. Zinner, Comparing models for the ground state energy of a trapped one-dimensional Fermi gas with a single impurity, J. Phys. B **49**, 125305 (2016).

[57] A. S. Dehkharghani, F. F. Bellotti, and N. T. Zinner, Analytical and numerical studies of Bose-Fermi mixtures in a one-dimensional harmonic trap, J. Phys. B **50**, 144002 (2017).

[58] F. F. Bellotti, A. S. Dehkharghani, and N. T. Zinner, Comparing numerical and analytical approaches to strongly interacting two-component mixtures in one dimensional traps, Eur. Phys. J. D **71**, 37 (2017).

[59] R. E. Barfknecht, I. Brouzos, and A. Foerster, Contact and static structure factor for bosonic and fermionic mixtures, Phys. Rev. A **91**, 043640 (2015).

[60] J. Chen, J. M. Schurer, and P. Schmelcher, Bunching-antibunching crossover in harmonically trapped few-body Bose-Fermi mixtures, Phys. Rev. A **98**, 023602 (2018).

[61] P. Siegl, S. I. Mistakidis, and P. Schmelcher, Many-body expansion dynamics of a Bose-Fermi mixture confined in an optical lattice, Phys. Rev. A **97**, 053626 (2018).

[62] S. Sachdev, *Quantum Phase Transitions* (Cambridge University Press, Cambridge, 2011).

[63] V. E. Korepin, N. M. Bogoliubov, and A. G. Izergin, *Quantum Inverse Scattering Method and Correlation Functions* (Cambridge University Press, Cambridge, 1993).

[64] F. H. L. Essler, H. Frahm, F. Göhmann, A. Klümper, and V. E. Korepin, *The One-Dimensional Hubbard Model* (Cambridge University Press, Cambridge, 2005).

[65] C. N. Yang and C. P. Yang, Thermodynamics of a one-dimensional system of bosons with repulsive delta-function interaction, J. Math. Phys. **10**, 1115 (1969).

[66] M. Takahashi, *Thermodynamics of One-Dimensional Solvable Models* (Cambridge University Press, Cambridge, 1999).

[67] C. N. Yang, Some Exact Results for the Many-Body Problem in One Dimension with Repulsive Delta-Function Interaction, Phys. Rev. Lett. **19**, 1312 (1967).

[68] M. Gaudin, Un systeme a une dimension de fermions en interaction, Phys. Lett. A **24**, 55 (1967).

[69] M. Suzuki, Transfer-matrix method and Monte Carlo simulation in quantum spin systems, Phys. Rev. B **31**, 2957 (1985).

[70] M. Suzuki and M. Inoue, The ST-transformation approach to analytic solutions of quantum systems. I: General formulations and basic limit theorems, Prog. Theor. Phys. **78**, 787 (1987).

[71] T. Koma, Thermal Bethe-Ansatz method for the one-dimensional Heisenberg model, Prog. Theor. Phys. **78**, 1213 (1987).

[72] J. Suzuki, Y. Akutsu, and M. Wadati, A new approach to quantum spin chains at finite temperature, J. Phys. Soc. Jpn. **59**, 2667 (1990).

[73] A. Klümper, Free energy and correlation lengths of quantum chains related to restricted solid-on-solid lattice models, Ann. Phys. (Leipzig) **504**, 540 (1992).

[74] A. Klümper, Thermodynamics of the anisotropic spin-1/2 Heisenberg chain and related quantum chains, Z. Phys. B **91**, 507 (1993).

[75] A. Klümper and O. I. Pâţu, Efficient thermodynamic description of multicomponent one-dimensional Bose gases, Phys. Rev. A **84**, 051604(R) (2011).

[76] O. I. Pâţu and A. Klümper, Thermodynamics, density profiles and correlation functions of the inhomogeneous one-dimensional spinor Bose gas, Phys. Rev. A **92**, 043631 (2015).

[77] O. I. Pâţu and A. Klümper, Thermodynamics, contact, and density profiles of the repulsive Gaudin-Yang model, Phys. Rev. A **93**, 033616 (2016).

[78] S. Tan, Energetics of a strongly correlated Fermi gas, Ann. Phys. (NY) **323**, 2952 (2008).

[79] S. Tan, Large momentum part of a strongly correlated Fermi gas, Ann. Phys. (NY) **323**, 2971 (2008).

[80] S. Tan, Generalized virial theorem and pressure relation for a strongly correlated Fermi gas, Ann. Phys. (NY) **323**, 2987 (2008).

[81] M. Olshanii and V. Dunjko, Short-Distance Correlation Properties of the Lieb-Liniger System and Momentum Distributions of Trapped One-Dimensional Atomic Gases, Phys. Rev. Lett. **91**, 090401 (2003).

[82] E. Braaten and L. Platter, Exact Relations for a Strongly Interacting Fermi Gas from the Operator Product Expansion, Phys. Rev. Lett. **100**, 205301 (2008).

[83] E. Braaten, D. Kang, and L. Platter, Exact Relations for a strongly interacting Fermi gas near a Feshbach resonance, Phys. Rev. A **78**, 053606 (2008).

[84] S. Zhang and A. J. Leggett, Universal properties of the ultracold Fermi gas, Phys. Rev. A **79**, 023601 (2009).

[85] R. Combescot, F. Alzetto, and X. Leyronas, Particle distribution tail and related energy formula, Phys. Rev. A **79**, 053640 (2009).

[86] F. Werner and Y. Castin, General relations for quantum gases in two and three dimensions: Two-component fermions, Phys. Rev. A **86**, 013626 (2012).

[87] F. Werner and Y. Castin, General relations for quantum gases in two and three dimensions. II. Bosons and mixtures, Phys. Rev. A **86**, 053633 (2012).

[88] M. Valiente, N. T. Zinner, and K. Mølmer, Universal relations for the two-dimensional spin-1/2 Fermi gas with contact interactions, Phys. Rev. A **84**, 063626 (2011).

[89] M. Valiente, N. T. Zinner, and K. Mølmer, Universal properties of Fermi gases in arbitrary dimensions, Phys. Rev. A **86**, 043616 (2012).

[90] M. Barth and W. Zwerger, Tan relations in one dimension, Ann. Phys. (NY) **326**, 2544 (2011).

[91] O. I. Pâţu and A. Klümper, Universal Tan relations for quantum gases in one dimension, Phys. Rev. A **96**, 063612 (2017).

[92] O. I. Pâţu, A. Klümper, and A. Foerster, Universality and Quantum Criticality of the One-Dimensional Spinor Bose Gas, Phys. Rev. Lett. **120**, 243402 (2018).

[93] E. H. Lieb and W. Liniger, Exact analysis of an interacting Bose gas. I. The general solution and the ground state, Phys. Rev. **130**, 1605 (1963).

[94] M. Takahashi, On the validity of collective variable description of Bose systems, Prog. Theor. Phys. **53**, 386 (1975).

[95] C. A. Tracy and H. Widom, On the ground state energy of the delta-function Bose gas, J. Phys. A: Math. Theor. **49**, 294001 (2016).

[96] S. Prolhac, Ground state energy of the δ-Bose and Fermi gas at weak coupling from double extrapolation, J. Phys. A: Math. Theor. **50**, 144001 (2017).

[97] G. Lang, F. Hekking, and A. Minguzzi, Ground-state energy and excitation spectrum of the Lieb-Liniger model: Accurate analytical results and conjectures about the exact solution, SciPost Phys. **3**, 003 (2017).

[98] V. V. Cheianov, H. Smith, and M. B. Zvonarev, Low-temperature crossover in the momentum distribution of cold atomic gases in one dimension, Phys. Rev. A **71**, 033610 (2005).

[99] A. Berkovich and J. H. Lowenstein, Correlation function of the one-dimensional Fermi gas in the infinite-coupling limit (repulsive case), Nucl. Phys. B **285**, 70 (1987).

[100] A. Berkovich, Temperature and magnetic field-dependent correlators of the exactly integrable (1+1)-dimensional gas of impenetrable fermions, J. Phys. A: Math. Gen. **24**, 1543 (1991).

[101] V. V. Cheianov and M. B. Zvonarev, Nonunitary Spin-Charge Separation in a One-Dimensional Fermion Gas, Phys. Rev. Lett. **92**, 176401 (2004).

[102] G. A. Fiete and L. Balents, Green's Function for Magnetically Incoherent Interacting Electrons in One Dimension, Phys. Rev. Lett. **93**, 226401 (2004).

[103] G. A. Fiete, *Colloquium:* The spin-incoherent Luttinger liquid, Rev. Mod. Phys. **79**, 801 (2007).

[104] Q. Zhou and T.-L. Ho, Signature of Quantum Criticality in the Density Profiles of Cold Atom Systems, Phys. Rev. Lett. **105**, 245702 (2010).

[105] F. He, Y. Jiang, Y.-C. Yu, H.-Q. Lin, and X.-W. Guan, Quantum criticality of spinons, Phys. Rev. B **96**, 220401(R) (2017).

[106] B. Yang, Y.-Y. Chen, Y.-G. Zheng, H. Sun, H.-N. Dai, X.-W. Guan, Z.-S. Yuan, and J.-W. Pan, Quantum Criticality and the Tomonaga-Luttinger Liquid in One-Dimensional Bose Gases, Phys. Rev. Lett. **119**, 165701 (2017).

[107] O. Breunig, M. Garst, A. Klümper, J. Rohrkamp, M. M. Turnbull, and T. Lorenz, Quantum criticality in the spin-1/2 Heisenberg chain system copper pyrazine dinitrate, Sci. Adv. **3**, eaao3773 (2017).

[108] Y.-C. Yu, Y.-Y. Chen, H.-Q. Lin, R. A. Römer, and X.-W. Guan, Dimensionless ratios: Characteristics of quantum liquids and their phase transitions, Phys. Rev. B **94**, 195129 (2016).

[109] X.-W. Guan, X.-G. Yin, A. Foerster, M. T. Batchelor, C.-H. Lee, and H.-Q. Lin, Wilson Ratio of Fermi Gases in One Dimension, Phys. Rev. Lett. **111**, 130401 (2013).

[110] Y. Maeda, C. Hotta, and M. Oshikawa, Universal Temperature Dependence of the Magnetization of Gapped Spin Chains, Phys. Rev. Lett. **99**, 057205 (2007).

[111] K. Ninios, T. Hong, T. Manabe, C. Hotta, S. N. Herringer, M. M. Turnbull, C. P. Landee, Y. Takano, and H. B. Chan, Wilson Ratio of a Tomonaga-Luttinger Liquid in a Spin-1/2 Heisenberg Ladder, Phys. Rev. Lett. **108**, 097201 (2012).

[112] S. Sachdev, T. Senthil, and R. Shankar, Finite-temperature properties of quantum antiferromagnets in a uniform magnetic field in one and two dimensions, Phys. Rev. B **50**, 258 (1994).

[113] J. Y. Lee, X. W. Guan, K. Sakai, and M. T. Batchelor, Thermodynamics, spin-charge separation, and correlation functions of spin-1/2 fermions with repulsive interaction, Phys. Rev. B **85**, 085414 (2012).

[114] J. H. H. Perk and C. L. Schultz, New families of commuting transfer matrices in q-state vertex models, Phys. Lett. A **84**, 407 (1981).

[115] C. L. Schultz, Eigenvectors of the multi-component generalization of the six-vertex model, Physica A **122**, 71 (1983).

[116] O. Babelon, H. J. de Vega, and C.-M. Viallet, Exact solution of the $Z_{n+1}\times Z_{n+1}$ symmetric generalization of the XXZ model, Nucl. Phys. B **200**, 266 (1982).

[117] H. J. de Vega, Yang-Baxter algebras, integrable theories and quantum groups, Int. J. Mod. Phys. A **4**, 2371 (1989).

[118] H. J. de Vega and E. Lopes, Exact Solution of the Perk-Schultz Model, Phys. Rev. Lett. **67**, 489 (1991).

[119] E. Lopes, Exact solution of the multi-component generalized six-vertex model, Nucl. Phys. B **370**, 636 (1992).

[120] A. Seel, T. Bhattacharyya, F. Göhmann, and A. Klümper, A note on the spin-1/2 XXZ chain concerning its relation to the Bose gas, J. Stat. Mech. (2007) P08030.

[121] B. Pozsgay, Local correlations in the 1D Bose gas from a scaling limit of the XXZ chain, J. Stat. Mech. (2011) P11017.

[122] O. I. Pâţu and A Klümper, Correlation lengths of the repulsive one-dimensional Bose gas, Phys. Rev. A **88**, 033623 (2013).

[123] E. T. Whittaker and G. N. Watson, *A Course of Modern Analysis* (Cambridge University Press, Cambridge, 1927), Sec. 6.3.

[124] F. Göhmann, Algebraic Bethe ansatz for the gl(1|2) generalized model and Lieb-Wu equations, Nucl. Phys. B **620**, 501 (2002).

[125] F. Göhmann and A. Seel, Algebraic Bethe ansatz for the gl(1|2) generalized model: II. The three gradings, J. Phys. A: Math. Gen. **37**, 2843 (2004).

[126] D. Arnaudon, N. Crampe, A. Doikou, L. Frappat, and E. Ragoucy, Spectrum and Bethe ansatz equations for the $\mathcal{U}_q(gl(\mathcal{N}))$ closed and open spin chains in any representation, Ann. Inst. Henri Poincare **7**, 1217 (2006).

[127] S. Belliard and E. Ragoucy, The nested Bethe ansatz for 'all' closed spin chains, J. Phys. A: Math. Theor. **41**, 295202 (2008).